Manipulating Skyrmion Motion on a Nanotrack with Varied Material Parameters and Tilted Spin Currents

Jia Luo(罗佳)[1], Jia-Hao Guo[2], Yun-He Hou(侯云鹤)[2], Jun-Lin Wang(王君林)[3,4], Yong-Bing Xu(徐永兵)[4], Yan Zhou(周艳)[5*], Philip Wing Tat Pong[6*], and Guo-Ping Zhao(赵国平)[1,7*]

[1]*College of Physics and Electronic Engineering, Sichuan Normal University, Chengdu 610068, China*
[2]*Department of Electrical and Electronic Engineering, The University of Hong Kong, Hong Kong, China*
[3]*School of Integrated Circuits, Guangdong University of Technology, Guangzhou 510006, China*
[4]*School of Physics, Engineering and Technology, University of York, York, YO10 5DD, United Kingdom*
[5]*School of Science and Engineering, The Chinese University of Hong Kong, Shenzhen 518172, China*
[6]*Department of Electrical and Computer Engineering, New Jersey Institute of Technology, NJ 07102, USA*
[7]*Center for Magnetism and Spintronics, Sichuan Normal University, Chengdu 610068, China*

(Received 6 July 2023; accepted manuscript online 28 August 2023)

Magnetic skyrmions are topological quasiparticles with nanoscale size and high mobility, which have potential applications in information storage and spintronic devices. The manipulation of skyrmion's dynamics in the track is an important topic due to the skyrmion Hall effect, which can deviate the skyrmions from the preferred direction. We propose a new model based on the ferromagnetic skyrmion, where the skyrmion velocity can be well controlled by adjusting the direction of the current. Using this design, we can avoid the annihilation of the skyrmion induced by the skyrmion Hall effect, which is confirmed by our micromagnetic simulation based on Mumax[3]. In the meantime, we increase the average velocity of the skyrmion by varying the intrinsic material parameters in the track, where the simulations agree well with our analytical results based on the Thiele equation. Finally, we give a phase diagram of the output of the skyrmion in the T-type track, which provides some practical ways for design of logic gates by manipulating crystalline anisotropy through the electrical control.

DOI: 10.1088/0256-307X/40/9/097501

Skyrmions were initially hypothesized in nuclear physics to characterize the resonance states of baryons,[1–7] which have been observed in a number of magnetic systems with broken inversion symmetries.[8,9] One kind of these systems, such as MnSi, $Fe_{1-x}Co_xSi$, and Cu_2OSeO_3 with the bulk Dzyaloshinskii–Moriya interaction (DMI), has a chiral crystal structure that supports skyrmions in the Bloch-type structure.[10–16] Another type of the system is ferromagnetic (FM) layer/heavy metal (HM) such as Fe/Ir,[17–19] Ni/Co,[20–22] and Ta/CoFeB/TaO_x,[23,24] which results in the interfacial DMI.[16,25] Due to the same topological form, a broad variety of magnetic configurations in the form of domain walls,[26–29] vortices,[30,31] bimeron,[32,33] and magnetic skyrmions have been intensely studied in magnetic materials in recent years. Furthermore, a magnetic skyrmion is a magnetic domain wall structure with topological protection in nanoscale.[34–36] As compared to magnetic domain walls, skyrmions have a small size on the order of 1 nm to 100 nm[37–39] and a low driven current density as low as 10^6 A/m^2.[40,41] Skyrmions are also one of the essential topological solitons in solid-state physics, and they are particularly important in the future applications of spintronics. They are anticipated to be one of the possible information carriers in future high-density data storage devices and information processing devices, such as spin torque oscillators,[42–45] logic gates,[4,46,47] and racetrack memories.[48–50]

According to these spintronic applications, the manipulation of skyrmions is crucial in order to address the growing need for information storage and processing technology.[34,51–53] The nucleation and stability of an isolated magnetic skyrmion, as well as the current-induced motion of magnetic skyrmions, have been thoroughly investigated so far.[54–56] In general, materials with strong spin-orbit interactions have large magnetic anisotropy. Since 2002, it has been demonstrated that perpendicular magnetic anisotropy (PMA)[57–60] exists at magnetic metal/oxide contacts. Subsequently, this PMA is observed in systems with moderate spin-orbit interactions, although its magnitude is equivalent to that measured at Co/Pt surfaces, a standard for substantial interfacial anisotropy.[61] In fact, this PMA was found to be rather common at magnetic metal/oxide interfaces, as it has been seen with a wide variety of amorphous or crystalline oxides.[62–65] A larger PMA can lead to a greater repulsive force because it generates an extra energy barrier that necessitates a higher current density to drive. In the meantime, the voltage was often used to modulate PMA constants in FM multilayer materials, which has been known as the voltage-controlled magnetic anisotropy (VCMA) effect.[48,66–68]

However, when driving the traditional ferromagnetic FM skyrmion with currents, due to the existence of the skyrmion Hall effect, the FM skyrmion will annihilate at the edge of the track causing signal loss. In order to overcome the skyrmion Hall effect, numerous solutions have been proposed. For example, researchers proposed

*Corresponding authors. Email: zhouyan@cuhk.edu.cn; philip.pong@njit.edu; zhaogp@uestc.edu.cn
© 2023 Chinese Physical Society and IOP Publishing Ltd

the synthetic antiferromagnetic (SAFM) skyrmion [69] and the antiferromagnetic (AFM) skyrmion;[70–72] high magnetic anisotropy K materials are added to the edge of the track.[73,74] In this Letter, a new model based on the FM skyrmion is proposed, in which we manipulate the direction of the skyrmion's velocity by adjusting the direction of the current. Using this method, we can avoid the annihilation of the skyrmion induced by the skyrmion Hall effect, which is confirmed by our micromagnetic simulation based on Mumax^3. In the meantime, we increase the average velocity of the skyrmion by varying the material parameters in some track areas, where the simulations agree well with our analytical results based on the Thiele equation. Finally, we give a phase diagram of the output of the skyrmion in the T-type track, which provides some practical ways for design of logic gates by manipulating crystalline anisotropy through the electrical control.

Method and Model. Spin-orbit torque (SOT) is used to drive FM skyrmion. Both the analytical calculation of the Thiele equation and the numerical simulation of Mumax^3 are based on the Landau–Lifshitz–Gilbert (LLG) equation driven by the electric current, which incorporates Slonczewski-like spin torques. The definition is as follows:[75,76]

$$\begin{aligned}\frac{d\boldsymbol{m}}{dt} =& -|\gamma|\boldsymbol{m}\times\boldsymbol{H}_{\text{eff}}+\alpha\Big(\boldsymbol{m}\times\frac{d\boldsymbol{m}}{dt}\Big)\\ &+|\gamma|\beta\epsilon\boldsymbol{m}\times(\boldsymbol{m}_{\text{p}}\times\boldsymbol{m})-|\gamma|\beta\epsilon'\boldsymbol{m}\times\boldsymbol{m}_{\text{p}},\end{aligned}\tag{1}$$

where $\boldsymbol{m}$ stands for the magnetization deduction M/M_{S}, and $\boldsymbol{H}_{\text{eff}}$ represents the effective field. The effective field $\boldsymbol{H}_{\text{eff}}$ includes exchange interactions, DMI, PMA, and dipole-dipole interaction (DDI); $\boldsymbol{m}_{\text{p}}$ is the polarization intensity vector; γ and α denote the gyromagnetic ratio and Gilbert damping constant, respectively. In the third term, $\beta=|\frac{\hbar}{2\mu_0 e}|\frac{j}{\tau M_{\text{S}}}$, where e is the electron charge in coulomb C, $\hbar$ is Planck's constant equal to 6.63×10^{-34} J·s, j denotes the current density in A/m^2, τ is the FM layer thickness in meter, and M_{S} is the saturation magnetization in A/m. In the last term, $\epsilon'=\xi\epsilon$, with ξ being the field-like SOT constant.

In this study, we use the Cartesian coordinate system, where the x, y, and z axes are along longitudinal, widthwise, and thickness directions of the track, respectively.

The indication of the skyrmion movement will be explained as the analysis of a modified Thiele equation under the assumption of the stiffness of spin textures. In this work, we consider an isolated Neél skyrmion in the presence of interfacial DMI. The skyrmion dynamics is well described in terms of the Thiele equation [4,77]

$$\boldsymbol{G}\times\boldsymbol{v}-\alpha\boldsymbol{D}_{\text{diss}}\cdot\boldsymbol{v}-\boldsymbol{F}_j=0.\tag{2}$$

The first term is the Magnus force with the gyrovector $\boldsymbol{G}=(4\pi Q\mu_0 M_{\text{S}}\tau/\gamma)\boldsymbol{e}_z$. It has been discovered that the Magnus force is proportional to the topological charge Q, which is an integer reflecting the number of times the spin direction wraps the unit sphere, i.e.,[78]

$$Q=-\frac{1}{4\pi}\int\big[\boldsymbol{m}\cdot(\partial_x\boldsymbol{m}\times\partial_y\boldsymbol{m})\big]dxdy,\tag{3}$$

where the number of topologies, Q, is ±1 for an isolated FM skyrmion. In Eq. (2), the second term describes the dissipative force, the dissipation tensor $\boldsymbol{D}_{\text{diss}}$ is given by

$$\boldsymbol{D}_{\text{diss}}=\frac{\mu_0 M_{\text{S}}\tau}{\gamma}\begin{pmatrix}d & 0\\ 0 & d\end{pmatrix},$$

with $d=\int(\partial_x\boldsymbol{m}\cdot\partial_x\boldsymbol{m})dxdy$. The third term $\boldsymbol{F}_j$ is the current-induced force that can be written as

$$\boldsymbol{F}_j=\frac{\mu_0 B_j M_{\text{S}}\tau}{\gamma}\begin{pmatrix}I_x\\ I_y\end{pmatrix},$$

with $B_j=\gamma\hbar m_{\text{p}}j/2\mu_0 e t_z M_{\text{S}}$ and $I_i=\int[(\boldsymbol{m}\times\hat{\boldsymbol{e}}_{\boldsymbol{m}_{\text{p}}})\cdot\partial_i\boldsymbol{m}]dxdy$, where m_{p} and $\hat{\boldsymbol{e}}_{\boldsymbol{m}_{\text{p}}}$ represent the value and direction of the polarization vector $\boldsymbol{m}_{\text{p}}$, respectively, i.e., $\boldsymbol{m}_{\text{p}}=m_{\text{p}}\hat{\boldsymbol{e}}_{\boldsymbol{m}_{\text{p}}}$.

For a typical SOT, the input current is in the HM layer along the film plane, which can induce the polarization current $\boldsymbol{j}$ in the HM layer through spin hall effect. In this case, $\boldsymbol{m}_{\text{p}}$ is perpendicular to $\boldsymbol{j}$ with both $\boldsymbol{m}_{\text{p}}$ and $\boldsymbol{j}$ in the plane of the film.[77] Further, by solving Eq. (2), we can obtain the velocity of the skyrmion in the directions of $\boldsymbol{j}$ and $\boldsymbol{m}_{\text{p}}$, expressed as[77]

$$v_{\boldsymbol{j}}=-\frac{\alpha d B_j I_x}{(4\pi Q)^2+\alpha^2 d^2},\tag{4}$$

$$v_{\boldsymbol{m}_{\text{p}}}=-\frac{4\pi Q B_j I_x}{(4\pi Q)^2+\alpha^2 d^2},\tag{5}$$

where $v_{\boldsymbol{j}}$ and $v_{\boldsymbol{m}_{\text{p}}}$ represent the velocity components in the directions of $\boldsymbol{j}$ and $\boldsymbol{m}_{\text{p}}$, respectively. The total velocity $\boldsymbol{v}=\sqrt{\boldsymbol{v}_{\boldsymbol{j}}^2+\boldsymbol{v}_{\hat{\boldsymbol{e}}\boldsymbol{m}p}^2}$ of the FM skyrmion, in this case, can also be obtained via $v_{\boldsymbol{j}}$ and $v_{\hat{\boldsymbol{e}}\boldsymbol{m}p}$. In the system studied here, the size of the skyrmion is about 10 nm, so d and I_x in Eqs. (4) and (5) can be approximated as[77] $d\approx2\pi[(R/\sqrt{A/K})+(\sqrt{A/K}/R)]$ and $I_x\approx\pi^2 R$, where R is the radius of the skyrmion. The R is related to the material parameters, which can be approximated as[79]

$$R\approx\frac{\sqrt{A/K}}{\sqrt{2-[\pi D/(2\sqrt{AK})]}}.\tag{6}$$

Now we can get the angle between the velocity $\boldsymbol{v}$ of the skyrmion and the current $\boldsymbol{j}$ by Eqs. (4) and (5), i.e., the Hall angle of the skyrmion θ_{SH}, which satisfies[80]

$$\tan\theta_{\text{SH}}=\frac{4\pi Q}{\alpha d}.\tag{7}$$

One can see that from Eq. (7), skyrmions will be deviated from the direction of the current by an angle θ_{SH}, which is called the skyrmion Hall effect in the literature, However, it has been rarely noticed that the direction of the skyrmion's velocity $\boldsymbol{v}$ can be adjusted by changing the current direction $\boldsymbol{j}$ so that the skyrmion can move in any direction we wanted. In particular, as we will show in the following, the annihilation of the skyrmion induced by the skyrmion Hall effect can be efficiently overcome if we design a suitable angle θ for the current $\boldsymbol{j}$.

In the micromagnetic simulation part, we use the Mumax^3 with the DMI extension module,[81] with the LLG equation governing the time-dependent magnetization dynamics. As shown in Fig. 1, the skyrmion motion in the FM layer is driven by the spin current generated due to the spin Hall effect in the HM layer. For simplicity, we directly simulate the injection of the spin-polarized current

with a certain current density and polarization rate. The polarization rate $m_{\rm p}$ of the spin current used in all simulations is 0.4. The structure is an ultrathin FM nanotrack on the HM with length $l = 500\,\text{nm}$ and width $w = 100\,\text{nm}$ with one modified PMA square area in the center of the nanotrack, with the length $a = 100\,\text{nm}$. The PMA value K_{uV} is controlled by applying voltage with a linearly varying relationship. The skyrmion will move on the FM free layer, and the interfacial DMI will be induced at the interface of the FM layer/HM layer. The starting location of the skyrmion is found at $x = 50\,\text{nm}$, $y = 0\,\text{nm}$, with the layer thickness set at 1 nm.

As shown in Fig. 1(b), an angle θ is assumed to be between the direction of the driven current and the longitudinal direction of the track to manipulate the skyrmion motion efficiently. Since the direction of polarization $\hat{\boldsymbol{e}}_{\boldsymbol{m}_{\rm p}}$ induced by the HM layer is always perpendicular to the direction of the current $\boldsymbol{j}$, the $\hat{\boldsymbol{e}}_{\boldsymbol{m}_{\rm p}}$ direction can be expressed as $\hat{\boldsymbol{e}}_{\boldsymbol{m}_{\rm p}} = (\sin\theta, \cos\theta, 0)$. We set the PMA constant K_{u0} in the center correction zone between $0.9K_u$ and $1.05K_u$, with $K_u = 0.8\,\text{MJ/m}^3$. The default magnetic parameters are adopted as follows:[78] the saturation magnetization $M_{\rm S} = 580 \times 10^3\,\text{A/m}$, the gyromagnetic ratio $\gamma = -2.211 \times 10^5\,\text{m/(A·s)}$, the Gilbert damping constant $\alpha = 0.1$, the current density $j = 4 \times 10^{11}\,\text{A/m}^2$, the PMA constant K, the exchange constant A, the DMI constant D. The discretization cell size is set as $1 \times 1 \times 1\,\text{nm}^3$.

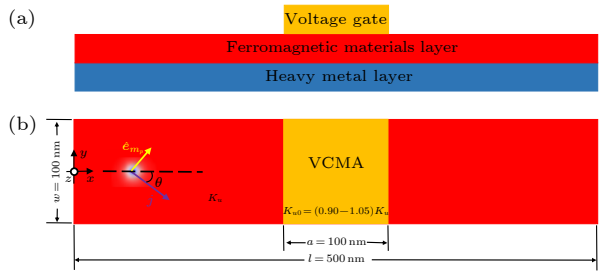

Fig. 1. (a) The simulated model of an FM skyrmion on an ultrathin FM/HM bilayer nanostructure. (b) The vertical view of the skyrmion motion on the nanotrack. The width $w = 100\,\text{nm}$, length $l = 500\,\text{nm}$, and the voltage-controlled-magnetic-anisotropy (VCMA) region length $a = 100\,\text{nm}$, in which a voltage gate K_{u0} is in the middle of the FM layer. The skyrmion is firstly located at $x = 50\,\text{nm}$ and $y = 0\,\text{nm}$. The $\hat{e}_{mp}$ and j indicate the polarization direction and the current direction, respectively, while θ represents the angle between $\hat{e}_{mp}$ and j. The PMA constant $K_u = 0.8\,\text{MJ/m}^3$ and $K_{u0} = 0.72$–$0.84\,\text{MJ/m}^3$, the exchange constant $A_u = A_{u0} = 15\,\text{pJ/m}$, the DMI constant $D_u = D_{u0} = 3.0\,\text{mJ/m}^2$.

Results and Discussions. Under the model in Fig. 1, we first perform a qualitative analysis of the motion of the skyrmion and infer the approximate range of skyrmion Hall angles. In the next model (Fig. 2), the relationship between the velocity and position of the skyrmion will be discussed in detail.

According to Eq. (6), an increase in the anisotropy constant K can reduce the skyrmion's radius, in the case of our parameters. By simulation, we confirm that when the PMA constant K_{u0} rises, the skyrmion's energy increases and its radius decreases. On the other hand, if the PMA constant goes down, the skyrmion's energy will decrease and its radius will increase. This phenomenon is consistent with the results in Ref. [82]. It can be seen from Eqs. (4) and (5) that the skyrmion velocity is roughly proportional to the skyrmion's radius for small α. Thus, the skyrmion velocity will rise when the PMA constant drops. Therefore, a larger PMA generates an energy barrier so that the skyrmion velocity will decrease, whereas a smaller PMA generates an energy trap where the skyrmion moves faster. The simulation results show that the radius R of the skyrmion is between 7 nm and 13 nm so that the dissipation constant d is between 14 and 21. According to Eq. (7), the $\tan\theta_{\rm SH}$ is between 5.99 and 8.8.

Now we can manipulate the skyrmion motion in the FM track freely, i.e., by changing θ, we can direct the skyrmion in any direction in the track we prefer. In particular, by designing a suitable angle θ, the skyrmion will move along the longitudinal direction of the track and will not annihilate by the skyrmion Hall effect. A close examination shows that the skyrmion's direction is not sensitive to the actual value of $\tan\theta$. Therefore, for convenience, we set $\tan\theta$ of the current in the entire HM to 6.0, as shown in Fig. 2(b). In the meantime, we can set up multiple PMA zones in the track and change the local speed of the skyrmion in the track to achieve a faster average speed. Figure 2 shows the design of the skyrmion racetrack with two voltage gates and a top view of the track of the skyrmion transmission through two PMA constants' regions controlled by voltage gates. The PMA constants of the two modified areas are K_{u1} and K_{u2}. Leaving the other parameters unchanged, we set K_{u1} and K_{u2} to $0.72\,\text{MJ/m}^3$ and $0.84\,\text{MJ/m}^3$, respectively.

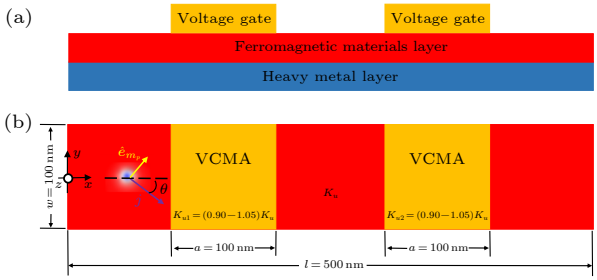

Fig. 2. (a) The simulated model of an FM skyrmion on an ultrathin FM/HM bilayer nanostructure. (b) The vertical view of the skyrmion motion on the nanotrack. The width $w = 100\,\text{nm}$, length $l = 500\,\text{nm}$, and the VCMA region length $a = 100\,\text{nm}$, where two voltage gates K_{u1} and K_{u2} are on the FM layer. The skyrmion is firstly located at $x = 50\,\text{nm}$ and $y = 50\,\text{nm}$. The PMA constant $K_u = 0.8\,\text{MJ/m}^3$, $K_{u1} = 0.72\,\text{MJ/m}^3$, and $K_{u2} = 0.84\,\text{MJ/m}^3$. The exchange constant $A_u = A_{u1} = A_{u2} = 15\,\text{pJ/m}$. The DMI constant $D_u = D_{u1} = D_{u2} = 3.0\,\text{mJ/m}^2$.

The simulation results with spatially varied crystalline anisotropy are shown in Fig. 3. The dotted line in Fig. 3(a) denotes the simulated velocity of the skyrmion as a function of position, where the speed of the skyrmion in the K_u area is maintained at about 100 m/s. When the skyrmion moves to the K_{u1} region, it encounters an energy trap and the velocity of the skyrmion rises to 155 m/s. As the skyrmion leaves the center of the K_{u1} region and moves towards the next K_u region, this energy trap will prevent it from leaving, slowing down the soliton's speed to about

100 m/s. As a whole, the K_{u1} region acts as an energy trap, which increases the average speed of the skyrmion. In contrary, when the skyrmion moves to the K_{u2} region, this area acts as an energy barrier so that the average velocity of the skyrmion will decrease. The velocity of the skyrmion can also be obtained by solving the Thiele equation, as shown by the red line in Fig. 3(a), which is in good agreement with the numerical data. Slightly larger differences occur near the boundary of the regions, i.e., $x = 100$ nm, 200 nm, 300 nm, and 400 nm, because we assume the ultrafast response of the skyrmion with the variation of the PMA in the analytical calculation. However, the actual change of the skyrmion speed will be delayed as it needs time to reach the stable speed. Figure 3(b) shows the trajectory of the skyrmion, indicating that the skyrmion is roughly along the x direction. As a result, our design of a tilted spin current as shown in Fig. 2 can avoid the annihilation of the skyrmion caused by the skyrmion Hall effect efficiently. It is noted, however, that there is a slight deviation from the x direction between $x = 50$–100 nm and 200–500 nm, which is due to the fact that the tilted angle is designed assuming $\tan\theta_{\rm SH} = 6.0$, whereas the actual $\tan\theta_{\rm SH}$ is between 6.0 and 8.8.

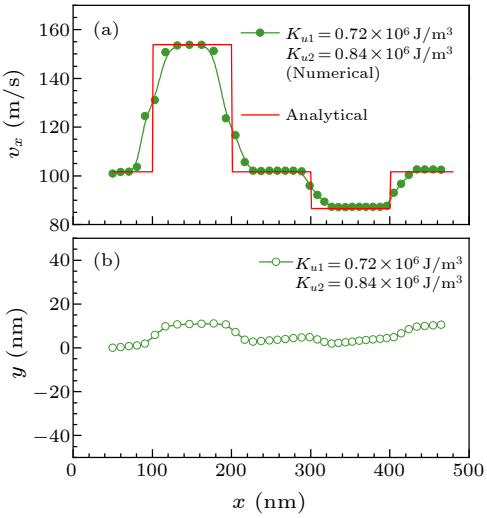

Fig. 3. (a) The skyrmion's velocity as a function of position. (b) The trajectory of the skyrmion. The parameters in (a) and (b) are $K_{u1} = 0.72 \times 10^6$ J/m^3, $K_{u2} = 0.84 \times 10^6$ J/m^3, $K_u = 0.80 \times 10^6$ J/m^3; $A_u = A_{u1} = A_{u2} = 15$ pJ/m; $D_u = D_{u1} = D_{u2} = 3.0$ mJ/m^2. The dotted lines and the solid red lines are the results of numerical simulation and analytical calculation, respectively.

We also investigate the effects of exchange interactions and DMI on skyrmion motion in Fig. 4, by changing the exchange constant and DMI constant locally. Both numerical and analytical results illustrate that a large DMI and a small A increase the velocity of the skyrmion, and vice versa, as shown in Figs. 4(a) and 4(c). According to Eq. (6), enhancement of DMI and reduction of A here play a similar role on the decrease of the PMA in the above case, which can increase the radius of the skyrmion and hence enlarge the skyrmion speed. In particular, one can see from Fig. 4(c) that a slight increase of D from 3.0 mJ/m^2 to 3.5 mJ/m^2, i.e., a 17% increase of D can enhance the skyrmion velocity by about 120%. On the other hand, the decreasing K and A have much smaller effects on the skyrmion speed. A close examination of Eq. (6) shows that the skyrmion size R is much more sensitive to the DMI value and hence explains the difference. Good agreement between numerical and analytical results justifies our explanation as well as our calculation. Similar to Fig. 3(b), Figs. 4(b) and 4(d) show that the skyrmions are roughly along the x direction, illustrating the effect of the tilted spin current in overcoming the annihilation of the skyrmion.

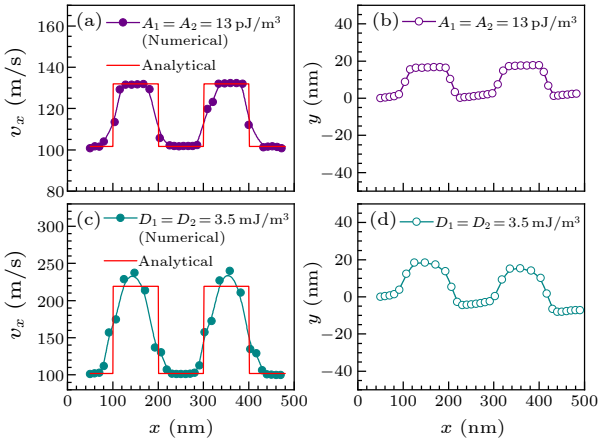

Fig. 4. (a) The skyrmion's velocity as a function of position. (b) The trajectory of the skyrmion. The parameters in (a) and (b) are $K_u = K_{u1} = K_{u2} = 0.80 \times 10^6$ J/m^3; $A_u = 15$ pJ/m, $A_{u1} = A_{u2} = 13$ pJ/m. (c) The skyrmion's velocity as a function of position. (d) The trajectory of the skyrmion. The parameters in (c) and (d) are $K_u = K_{u1} = K_{u2} = 0.80 \times 10^6$ J/m^3; $A_u = A_{u1} = A_{u2} = 15$ pJ/m; $D_u = 3.0$ mJ/m^2, $D_{u1} = D_{u2} = 3.5$ mJ/m^2. The dotted lines and the solid red lines are the results of numerical simulation and analytical calculation, respectively.

Using varied anisotropy and the tilted spin current, we can design a T-type track for magnetic skyrmion motion on nanomaterials. As illustrated in Fig. 5(a), the skyrmion is initially placed on the top left of the T-type track, where the PMA constants in the K_{u4} area and the K_{u3} area can vary.

First of all, as shown in Fig. 5(b), we give the phase diagram of the motion of skyrmion with different tilted angles in the T-type track. From Fig. 5(b), we can see that there are three types of skyrmion motion, namely annihilation, entering the K_{u4} region, and turning right into the lower K_{u3} region. For convenience, we denote the two states of "entering the K_{u4} region" and "entering the lower K_{u3} region" as state "0" and state "1", respectively. When the tilted angle of the current is between 70° and 90°, the skyrmion will be in state 0. Increase of the tilted angle of the current to 100° will change the skyrmion state to 1. This remains for the angle below 110°. Further, when the tilted angle of the current is larger than 110° or smaller than 70°, the skyrmion will annihilate. Interestingly, we can see that the state of the skyrmion is unchanged for various anisotropy constants K of the T-type track, indicating the stability of the present design of the logic gate.

Furthermore, based on the results in Fig. 5(b), we im-

prove the design of the ordinary VCMA control skyrmion by adding a constant to the tilted angles of the current $\theta = 90°$. We consider the joint effect of skyrmion motion directions by adjusting PMA constants in K_{u3} and K_{u4} regions, with results shown in Fig. 5(c). The skyrmion motion on the FM layer shows two scenarios, including outputting data "0", which indicates that the skyrmion goes into the K_{u4} region and outputting data "1", which denotes that the skyrmion will alter its motion direction and turn right into the lower K_{u3} region. The phase boundary of two motion statuses shows the step shape, where the final position of the skyrmion is determined by the difference in parameters between the two regions. The smaller the difference between K_{u3} and K_{u4}, the smaller the energy difference in the two regions, and hence the easier the passage of the skyrmion from the left to the right. The tilted spin current here avoids the annihilation of skyrmion signals caused by the skyrmion Hall effect, and facilitates the manipulation of the skyrmion.

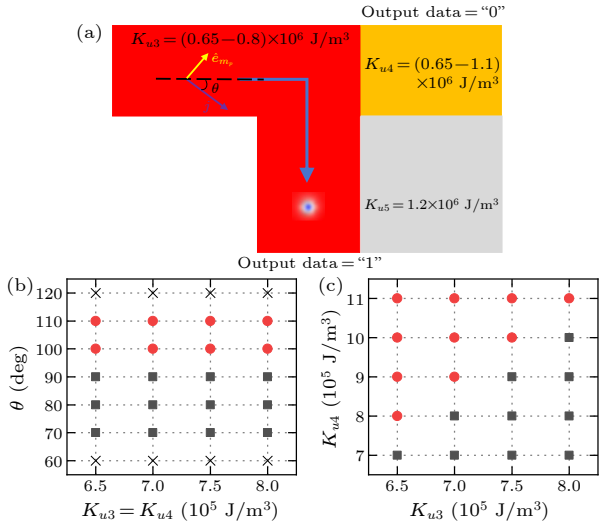

Fig. 5. (a) The track model of T-type. (b) Phase diagram of the motion of skyrmion with different tilted angles. (c) Phase diagrams of the motion of skyrmion with various (a) PMA constants K_{u3} and K_{u4}. We fix PMA constant $K_{u5} = 1.2\times10^6$ J/m^3, exchange energy constant $A = 15.0\times10^{-12}$ J/m and DMI constants $D = 3.0$ mJ/m^2. In (b) and (c), the ×, red dots, and black squares denote annihilation, state 1, and state 0, respectively.

Compared with the design of existing spintronic devices,[4,42–50,73,74] our design is also to guide the skyrmion's motion by changing the energy potential. However, our design can manipulate the output of the device by adjusting the angle of the current, as shown in Fig. 5(b). In comparison to the method of VCMA manipulation skyrmion, our method removes the complex voltage control step and can realize the output of signal 0 or 1 by simply adjusting the current. In addition, under different parameters K, the output results of this method are basically unchanged and relatively stable. Therefore, our design is simpler and easily to be realized in the experiment. Further, according to the results of Fig. 5(c), our design can also have the functions of the original VCMA device. In summary, the present design can realize the control of the output signal from two ways, by adjusting the current in the plane and manipulating the VCMA out of the plane. Our results here open a new route for the efficient manipulation of skyrmions and the construction of skyrmion-based spintronics devices.

In conclusion, we have proposed a new model based on the FM skyrmion, which allows for the manipulation of the skyrmion's velocity direction by adjusting the current direction. This approach enables the skyrmion to move in any desired direction, where we have increased the average velocity of the skyrmion by modifying the material parameters in specific track areas. A large PMA, a large DMI, or a small A can increase the velocity of the skyrmion by increasing its radius, within the parameters considered here. Moreover, we find that the skyrmion's size and speed are more sensitive to DMI than to PMA and exchange interactions. The simulation results agree well with the analytical results based on the Thiele equation. In addition, we design a T-type track using varied anisotropy and a tilted spin current and provided a phase diagram, where we can control the skyrmion's trajectory by adjusting the current direction or the PMA in different regions. Overall, our findings suggest that the control of skyrmion dynamics can be achieved by adjusting material parameters and designing specific track geometries. Further research is necessary to explore the full potential of these approaches and their practical applications.

Acknowledgments. This work was supported by the National Natural Science Foundation of China (Grant Nos. 51771127, 52171188, 52111530143, 11974298, 12374123, and 12241403), the Central Government Funds of Guiding Local Scientific and Technological Development of Sichuan Province (Grant No. 2021ZYD0025), the Shenzhen Fundamental Research Fund (Grant No. JCYJ20210324120213037), Shenzhen Peacock Group Plan (Grant No. KQTD20180413181702403), the Key-Area Research & Development Program of Guangdong Province (Grant No. 2021B0101300003), and the Guangdong Basic and Applied Basic Research Foundation (Grant Nos. 2022A1515110863 and 2023A1515010837).

References

[1] Fert A, Reyren N, and Cros V 2017 *Nat. Rev. Mater.* **2** 17031
[2] Tokura Y and Kanazawa N 2021 *Chem. Rev.* **121** 2857
[3] Zhang X C, Zhou Y, Song M K, Park T E, Xia J, Ezawa M, Liu X, Zhao W, Zhao G P, and Woo S 2020 *J. Phys.: Condens. Matter* **32** 143001
[4] Zhang X C, Ezawa M, and Zhou Y 2015 *Sci. Rep.* **5** 9400
[5] Roessler K U, Bogdanov A, and Pfleiderer C 2006 *Nature* **442** 797
[6] Weidig T 1999 *Nonlinearity* **12** 1489
[7] Ball R 1990 *Int. J. Mod. Phys. A* **5** 4391
[8] Jiang W, Chen G, Liu K, Zang J, Te G S, and Hoffmann A 2017 *Phys. Rep.* **704** 1
[9] Mühlbauer S, Binz B, Jonietz F, Pfleiderer C, Rosch A, Neubauer A, Georgii R, and Böni P 2009 *Science* **323** 915
[10] Di K, Zhang L V, Lim S H, Ng C S, Kuok H M, Yu J, Yoon J, Qiu X, and Yang H 2015 *Phys. Rev. Lett.* **114** 47201
[11] El H S, Bailly-Reyre A, and Diep H 2018 *J. Magn. Magn. Mater.* **455** 32
[12] Jaiswal S, Litzius K, Lemesh I, Büttner F, Finizio S, Raabe J, Weig M, Lee K, Langer J, and Ocker B 2017 *Appl. Phys. Lett.* **111** 22409

[13] Ryu K S, Thomas L, Yang S H, and Parkin 2013 *Nat. Nanotechnol.* **8** 527
[14] Sergienko A I and Dagotto E 2006 *Phys. Rev. B* **73** 94434
[15] Zhou Y, Mansell R, Valencia S, Kronast F, and van Dijken S 2020 *Phys. Rev. B* **101** 54433
[16] Yang H X, Liang J H, and Cui Q R 2023 *Nat. Rev. Phys.* **5** 43
[17] Soumyanarayanan A, Raju M, Oyarce G A, Tan K A, Im M Y, Petrović A, Ho P, Khoo K, Tran M, and Gan C 2017 *Nat. Mater.* **16** 898
[18] Raju M, Yagil A, Soumyanarayanan A, Tan K A, Almoalem A, Ma F, Auslaender O M, and Panagopoulos C 2019 *Nat. Commun.* **10** 696
[19] Hagemeister J, Iaia D, Vedmedenko Y E, von Bergmann K, Kubetzka A, and Wiesendanger R 2016 *Phys. Rev. Lett.* **117** 207202
[20] Li M, Lau D, De Graef M, and Sokalski V 2019 *Phys. Rev. Mater.* **3** 64409
[21] Brock A J, Montoya A S, Im M Y, and Fullerton E E 2020 *Phys. Rev. Mater.* **4** 104409
[22] Hrabec A, Sampaio J, Belmeguenai M, Gross I, Weil R, Chérif M S, Stashkevich A, Jacques V, Thiaville A, and Rohart S 2017 *Nat. Commun.* **8** 15765
[23] Syamlal S, Kalal S, Perumal P H, Kumar D, Gupta M, and Sinha J 2021 *Mater. Sci. Eng. B* **272** 115367
[24] Ojha B, Mallick S, Sharma M, Thiaville A, Rohart S, and Bedanta S 2021 Xiv:2106.2407 [cond-mat.mtrl-sci]
[25] Wang Z W, Liang J H, and Yang H X 2023 *Chin. Phys. Lett.* **40** 017501
[26] Allwood A D, Xiong G, Faulkner C, Atkinson D, Petit D, and Cowburn R 2005 *Science* **309** 1688
[27] Franken H J, Herps M, Swagten J H, and Koopmans B 2014 *Sci. Rep.* **4** 5248
[28] Luo Z, Hrabec A, Dao P T, Sala G, Finizio S, Feng J, Mayr S, Raabe J, Gambardella P, and Heyderman J L 2020 *Nature* **579** 214
[29] Parkin S S, Hayashi M, and Thomas L 2008 *Science* **320** 190
[30] Papanicolaou N and Tomaras T 1991 *Nucl. Phys. B* **360** 425
[31] Ivanov B, Stephanovich V, and Zhmudskii A 1990 *J. Magn. Magn. Mater.* **88** 116
[32] Göbel B, Mook A, Henk J, Mertig I, and Tretiakov A O 2019 *Phys. Rev. B* **99** 60407
[33] Shen L C, Xia J, Zhang X C, Ezawa M, Tretiakov A O, Liu X, Zhao G P, and Zhou Y 2020 *Phys. Rev. Lett.* **124** 37202
[34] Je G S, Han H S, Kim K S, Montoya A S, Chao W, Hong I S, Fullerton E E, Lee K S, Lee K J, and Im M Y 2020 *ACS Nano* **14** 3251
[35] Liang D, DeGrave P J, Stolt J M, Tokura Y, and Jin S 2015 *Nat. Commun.* **6** 8217
[36] Wild J, Meier N T, Pöllath S, Kronseder M, Bauer A, Chacon A, Halder M, Schowalter M, Rosenauer A, and Zweck J 2017 *Sci. Adv.* **3** e1701704
[37] Wang X, Yuan H, and Wang X 2018 *Commun. Phys.* **1** 31
[38] Wu H, Hu X, Jing K, and Wang X 2021 *Commun. Phys.* **4** 210
[39] Liu J H, Wang Z D, Xu T, Zhou H A, Zhao L, Je S G, Im M Y, Fang L, and Jiang W J 2022 *Chin. Phys. Lett.* **39** 017501
[40] Yu X, Kanazawa N, Zhang W, Nagai T, Hara T, Kimoto K, Matsui Y, Onose Y, and Tokura Y 2012 *Nat. Commun.* **3** 988
[41] Juge R, Je S G, de Souza D, Buda-Prejbeanu D L, Peña-Garcia J, Nath J, Miron M I, Rana G K, Aballe L, and Foerster M 2019 *Phys. Rev. Appl.* **12** 44007
[42] Garcia-Sanchez F, Sampaio J, Reyren N, Cros V, and Kim J 2016 *New J. Phys.* **18** 75011
[43] Guo J, Xia J, Zhang X C, WP P, Wu Y, Chen H, Zhao W, and Zhou Y 2020 *J. Magn. Magn. Mater.* **496** 165912
[44] Zhang S, Wang J, Zheng Q, Zhu Q, Liu X, Chen S, Jin C, Liu Q, Jia C, and Xue D 2015 *New J. Phys.* **17** 23061
[45] Jin Z N, Song M H, Fang H N, Chen L, Chen J W, and Tao Z K 2022 *Chin. Phys. Lett.* **39** 108502
[46] Luo S, Song M, Li X, Zhang Y, Hong J, Yang X, Zou X, Xu N, and You L 2018 *Nano Lett.* **18** 1180
[47] Yu D X, Yang H X, Chshiev M, and Fert A 2022 *Natl. Sci. Rev.* **9** nwac021
[48] Kang W, Huang Y, Zheng C, Lv W, Lei N, Zhang Y, Zhang X C, Zhou Y, and Zhao W 2016 *Sci. Rep.* **6** 23164
[49] Kang W, Zheng C, Huang Y, Zhang X C, Zhou Y, Lv W, and Zhao W 2016 *IEEE Electron Device Lett.* **37** 924
[50] Zhang X C, Zhao G P, Fangohr H, Liu P J, Xia W, Xia J, and Morvan F 2015 *Sci. Rep.* **5** 7643
[51] Li X and Yang J 2013 *Phys. Chem. Chem. Phys.* **15** 15793
[52] Wang Z, Guo M, Zhou H A, Zhao L, Xu T, Tomasello R, Bai H, Dong Y, Je S G, and Chao W 2020 *Nat. Electron.* **3** 672
[53] Yang H, Wang F, Zhang H S, Guo L H, Hu L Y, Wang L F, Xue D J, and Xu X H 2020 *J. Am. Chem. Soc.* **142** 4438
[54] Zhang X C, Zhou Y, and Ezawa M 2016 *Sci. Rep.* **6** 24795
[55] Sampaio J, Cros V, Rohart S, Thiaville A, and Fert A 2013 *Nat. Nanotechnol.* **8** 839
[56] Zázvorka J, Jakobs F, Heinze D, Keil N, Kromin S, Jaiswal S, Litzius K, Jakob G, Virnau P, and Pinna D 2019 *Nat. Nanotechnol.* **14** 658
[57] Zhang H S, Qin W, Chen M X,Cui P, Zhang Z Y and Xu X H 2019 *Phys. Rev. B* **99** 165410
[58] Guo J, Xia J, Zhang X C, Pong W P, and Zhou Y 2021 *Phys. Lett. A* **392** 127157
[59] Sbiaa R, Meng H, and Piramanayagam S 2011 *Phys. Status Solidi RRL* **5** 413
[60] Zhang H S, Yang W J, Ning YH and Xu X H 2020 *Phys. Rev. B* **101** 205404
[61] Carcia P 1988 *J. Appl. Phys.* **63** 5066
[62] Carcia P, Meinhaldt A, and Suna A 1985 *Appl. Phys. Lett.* **47** 178
[63] Daalderop G, Kelly P, and Den Broeder F 1992 *Phys. Rev. Lett.* **68** 682
[64] Den Broeder F, Kuiper D, de Van A, and Hoving W 1988 *Phys. Rev. Lett.* **60** 2769
[65] Iwasaki I S and Ouchi K 1978 *IEEE Trans. Magn.* **14** 849
[66] Wang K L, Alzate J G, and Amiri P K 2013 *J. Phys. D* **46** 074003
[67] Liu Y, Lei N, Wang C, Zhang X C, Kang W, Zhu D, Zhou Y, Liu X, Zhang Y, and Zhao W 2019 *Phys. Rev. Appl.* **11** 14004
[68] Nozaki T, Shiota Y, Shiraishi M, Shinjo T, and Suzuki Y 2010 *Appl. Phys. Lett.* **96** 022506
[69] Zhang X C, Yan Z, and Ezawa M 2016 *Nat. Commun.* **7** 10293
[70] Shen L C, Li X G, Zhao Y L, Xia J, Zhao G P, and Yan Z 2019 *Phys. Rev. Appl.* **12** 064033
[71] Liang X, Zhao G P, Shen L C, Xia J, Zhang X C, and Zhou Y 2019 *Phys. Rev. B* **100** 144439
[72] Qi S F, Qiao Z H, Deng X Z, Cubuk E D, Chen H, Zhu W G, Kaxiras E, Zhang S B, Xu X H, and Zhang Z Y 2016 *Phys. Rev. Lett.* **117** 056804
[73] Lai P, Zhao G P, Tang H, Ran N, Wu S Q, Xia J, Zhang X C, and Zhou Y 2017 *Sci. Rep.* **7** 45330
[74] Zhang X C, Ezawa M, Xiao D, Zhao G P, Liu Y, and Zhou Y 2015 *Nanotechnology* **26** 225701
[75] Bartels S, Ko J, and Prohl A 2008 *Math. Comput.* **77** 773
[76] Nakatani Y, Uesaka Y, and Hayashi N 1989 *Jpn. J. Appl. Phys.* **28** 2485
[77] Shen L C, Xia J, Zhao G P, Zhang X C, Ezawa M, Tretiakov O A, Liu X X, and Zhou Y 2019 *Appl. Phys. Lett.* **114** 042402
[78] Yin G, Li Y, Kong L, Lake K R, Chien C L, and Zang J 2016 *Phys. Rev. B* **93** 174403
[79] Rohart S and Thiaville A 2013 *Phys. Rev. B* **88** 184422
[80] Zhang X C, Xia J, and Liu X X 2022 *Phys. Rev. B* **106** 094418
[81] Arne V, Jonathan L, Mykola D, Mathias H, Felipe F G, and Bartel V W 2014 *AIP Adv.* **4** 107133
[82] Mehmood N, Wang J B, Zhang C L, Zeng Z Z, Wang J N, and Liu Q F 2022 *J. Magn. Magn. Mater.* **545** 168775